Conserved and derived expression patterns and positive selection on dental genes reveal complex evolutionary context of ever-growing rodent molars

AUTHORS:

Zachary T. Calamari[1,2,3,4,*], zachary.calamari@baruch.cuny.edu

Andrew Song[1,5], ajs557@cornell.edu

Emily Cohen[1,6], ec4744@nyu.edu

Muspika Akter[1], muspika.akter@baruchmail.cuny.edu

Rishi Das Roy[7], rishi.dasroy@helsinki.fi

Outi Hallikas[7], outi.hallikas@helsinki.fi

Mona M. Christensen[7], mona.christensen@helsinki.fi

Pengyang Li[3,8], pengyang.li@cshs.org

Pauline Marangoni[3,8], pauline.marangoni@cshs.org

Jukka Jernvall[7,9], jernvall@fastmail.fm

Ophir D. Klein[3,8,*] ophir.klein@cshs.org

[1]Baruch College, City University of New York, One Bernard Baruch Way, New York, NY 10010, USA

[2]The Graduate Center, City University of New York, 365 Fifth Ave, New York, NY 10016, USA

[3]Program in Craniofacial Biology and Department of Orofacial Sciences, University of California, San Francisco, San Francisco, CA 94158, USA

[4]Division of Paleontology, American Museum of Natural History, Central Park West at 79th Street, New York, NY, 10024, USA

[5]Cornell University, 616 Thurston Ave, Ithaca, NY 14853, USA

[6]New York University College of Dentistry, 345 E 34th St, New York, NY 10010

[7]Institute of Biotechnology, University of Helsinki, FI-00014 Helsinki, Finland

[8]Department of Pediatrics, Cedars-Sinai Guerin Children's, 8700 Beverly Blvd., Suite 2416, Los Angeles, CA 90048, USA

[9]Department of Geosciences and Geography, University of Helsinki, FI-00014 Helsinki, Finland

*Corresponding authors

ABSTRACT

Background: Continuously growing teeth are an important innovation in mammalian evolution, yet genetic regulation of continuous growth by stem cells remains incompletely understood. Dental stem cells are lost at the onset of tooth root formation, but this loss of continuous crown growth is difficult to study in the mouse because regulatory signaling overlaps with signals that pattern tooth size and shape. Within the voles (Cricetidae, Rodentia, Glires), species have evolved both rooted and unrooted molars that have similar size and shape. We assembled a *de novo* genome of *Myodes glareolus*, a vole with high-crowned, rooted molars, and performed genomic and transcriptomic analyses in a broad phylogenetic context of Glires (rodents and lagomorphs) to assess differential selection and evolution in tooth forming genes.

Results: Our *de novo* genome recovered 91% of single-copy orthologs for Euarchontoglires and had a total length of 2.44 Gigabases, enabling genomic and transcriptomic analyses. We identified six dental genes undergoing positive selection across Glires and two genes undergoing positive selection in species with unrooted molars, *Dspp* and *Aqp1*. Transcriptomics analyses

demonstrated conserved patterns of dental gene expression with species-specific variation likely related to developmental timing and morphological differences between mouse and vole molars. *Conclusions:* Our results support ongoing dental gene evolution in rodents with unrooted molars. We identify candidate genes for further functional analyses, particularly *Dspp*, which plays an important role in mineralizing tissues. Our expression results support conservation of dental genes between voles and model species like mice, while revealing significant effects of overall tooth morphology on gene expression.

3-10 Keywords: Evolution, selection, Glires, molar, root, dental, development, genome, rodent, tooth

DECLARATIONS

Ethics approval: The University of California, San Francisco (UCSF) Institutional Animal Care and Use Program and the Finnish national animal experimentation board approved protocols for humane euthanasia and collection of tissues for animals used in this study under protocols AN189916 (UCSF) and KEK16-021, KEK19-019, and KEK17-030 (University of Helsinki).

Consent for publication: Not applicable.

Availability of data and materials: The datasets supporting the conclusions of this article are available in the GenBank repository under [GenBank reference number to be added upon acceptance] and in the article's additional files.

Competing interests: The authors declare that they have no competing interests.

Funding: This research was supported by National Science Foundation grants CNS-0958379, CNS-0855217, OAC-1126113, and OAC-2215760 through the City University of New York High Performance Computing Center at the College of Staten Island; OAC-1925590 through the MENDEL high performance computing cluster at the American Museum of Natural History; Academy of Finland to JJ; Doctoral Programme in Biomedicine, University of Helsinki to MMC; and National Institutes of Health NIDCR R01-DE027620 and R35-DE026602 to ODK.

Authors' contributions: ZTC and ODK designed the study. ZTC and PM performed animal husbandry. ZTC performed and oversaw tissue sampling, sequencing, genome assembly and annotation for *Myodes glareolus*. ZTC, AS, JR, EC, and MA performed genome computational analyses. PL performed qPCR analyses. OH, MMC, RDR, and JJ designed and implemented RNA sequencing experiments. ZTC wrote and all authors contributed to and approved the manuscript.

Acknowledgements: The authors thank A. Joo, N. Ahituv, G. Amato, A. Narechania, S. Singh, A. Scott, and A. Paasch for advice on methods and access to cluster computing resources.

BACKGROUND

Hypselodonty, or the presence of unrooted and thus ever-growing teeth, has evolved multiple times in mammals. Glires—the clade containing rodents, rabbits, and their relatives—have hypselodont incisors (1), and multiple Glires have also evolved hypselodont molars (Fig.

1). At least in rodents, molar hypselodonty evolved considerably later than hypsodont molars, which are high crowned but rooted, which in turn evolved later than hypselodont incisors. In Glires, molars appear to increase in crown height from low-crowned brachydont (low-crowned, rooted), through hypsodonty (high-crowned, rooted), toward hypselodonty (high-crowned, unrooted) (2). Mice (*Mus musculus*), the primary mammalian model species of dental research, have highly derived hypselodont incisors while retaining brachydont molars. Because of this, mice do not provide information about the hypsodont teeth that likely preceded hypselodonty.

Mammalian teeth sit in bony sockets, held in place by soft tissue (periodontal ligament) attached to cementum-covered tooth roots (3). Ligamentous tooth attachment may have arisen along with a reduction in the rate of tooth replacements, providing greater flexibility for repositioning the teeth as the dentary grows (4,3). Consequently, the limited replacement of mammalian teeth (two sets of teeth in most mammals and one in Glires) may have spurred the evolution of hypsodont and hypselodont teeth, both with high crowns that compensate for tooth wear from gritty or phytolith-heavy diets (5,6), and resulted in further modification of the anchoring roots. The convergent evolution of unrooted molars in Glires presents an opportunity to identify whether consistent developmental and genomic changes underlie the formation of hypselodont teeth, in turn revealing the mechanisms that must remain unchanged to produce tooth roots. Furthermore, the relatively recent evolution of molar hypselodonty, starting in the Middle Miocene (approximately 16-12 Ma) (2), should provide molecular evidence for the steps required to make a continuously growing organ.

Dental development proceeds from the tooth germ, composed of epithelium and mesenchyme, through phases known as the bud, cap, and bell (7). Multipotent enamel epithelium differentiates into the cells that form the tooth crown (8–11). As development progresses in

rooted teeth, the epithelium at the tooth apex transitions first to a tissue called Hertwig's epithelial root sheath (HERS), and eventually cementum-covered roots (9,10). Studies have identified numerous candidate genes and pathways with various roles during root development, such as *Fgf10*, which decreases in expression at the beginning of root formation (12–18). Although research on mouse molars has identified genetic signals of root formation, a number of the key genes studied have broad developmental roles, such as *Wnt* family members (14), or overlap considerably with genes also involved in patterning the size and shape of the tooth (17,19–22). This overlap between shape and root expression patterns confounds our ability to identify a clear signal initiating root formation.

Evolutionary novelties such as high-crowned hypsodont and hypselodont molars can arise from differences in gene expression and regulation (23–26). Evolutionarily conserved gene expression levels produce conserved phenotypes, and changes in gene regulatory networks have long been linked to morphological evolution (27,28). The order of genes along a chromosome (synteny) can affect gene expression and regulation, as regulatory sequences are often located near their target genes (cis-regulatory elements) (29–31). Genome rearrangements that place genes near new regulatory elements may result in changes of the expression levels and selective environment of those genes; these small-scale rearrangements of genes may be common in mammals (32–34). Genes involved in molar development are not syntenic in the mouse genome nor are genes with organ-specific expression (35), and thus the regulatory effects of co-localization need not apply to all dental genes at once. Changes in genome architecture between Glires species thus may result in different selective and expression environments for dental genes that could result in the evolution of hypselodont molars.

To establish a model rodent species with hypsodont molars for close comparison to hypselodont molars, we sequenced and annotated a highly-complete *de novo* genome of *Myodes glareolus*, the bank vole. The bank vole is increasingly used in medical and environmental research, ranging from studying zoonotic diseases (36) to immune responses (37,38), and even assessing environmental remediation efforts through heavy metals that accumulate in vole teeth (39,40), thus our efforts may be of use beyond dental research. The bank vole's hypsodont molars bridge the gap between low-crowned mouse and hypselodont prairie vole (*Microtus ochrogaster*) molars. We performed a suite of genomic and transcriptomic tests of our new bank vole genome in a broad phylogenetic context to test the hypothesis that dental genes are undergoing positive selection and exhibit different expression patterns in species with unrooted, hypselodont molars. We predicted that genes without conserved syntenic relationships in these species would be more likely to have sites under positive selection or significantly different expression. Our analyses revealed positive selection among two dental genes in Glires with unrooted molars compared to those with rooted molars and demonstrated strong conservation of dental gene expression patterns between bank voles and mice, with key differences related to the timing and patterning of tooth morphology.

RESULTS

Orthology and synteny analyses

To identify which sequences in our bank vole (*Myodes glareolus*) genome and annotation had the same evolutionary history as dental genes identified in other Glires and assess genome rearrangements, we performed orthology and synteny analyses in a broad phylogenetic context. OrthoFinder identified 20,547 orthogroups representing 97.9% of the genes across all 24 analyzed genomes (including the human outgroup). Of the orthogroups, 6,158 had all species

present. In our *de novo* bank vole genome, there were 27,824 annotated genes, of which 84.2% were assigned to an orthogroup. Bank vole genes were present in 16,250 orthogroups. On average, the genomes included in the OrthoFinder analysis had 19,814 genes, with 98.2% of those assigned to orthogroups.

The completeness and large scaffold N50 (4.6 Megabases) of our bank vole assembly supported its inclusion in generating a Glires synteny network. Using the infomap clustering algorithm, we produced 19,694 microsynteny clusters from this overall synteny network. We did not expect dental genes to share the same microsynteny cluster, and instead examined whether each gene was in the same microsynteny cluster in species with rooted or unrooted molars. Among the microsynteny clusters containing dental genes, 28 networks lacked synteny in at least half the species with unrooted molars or did not have a one-to-one relationship with an orthogroup (Fig. 2).

Positive selection analysis

We hypothesized that dental genes in species with unrooted molars are undergoing positive selection. Our positive selection analyses in PAML (phylogenetic analysis by maximum likelihood (41)) identified 6 dental gene orthogroups undergoing site-specific positive selection across Glires (Table 1). One of these genes, *Col4a1*, also was largely not syntenic in species with unrooted molars (Fig. 2). Another orthogroup consisted mainly of predicted sequences similar to *Runx3* but only had sequences from four species; both showed site-specific positive selection. We then assessed 24 genes (those with site-specific positive selection or which lacked synteny in at least half of the species with unrooted molars) for site-specific positive selection in species with unrooted molars compared to species with rooted molars (branch-and-site specific positive

selection (42)). Two genes, *Dspp* and *Aqp1* were undergoing this branch-and-site specific positive selection. Both genes had a single highly supported site (posterior probability > 0.95) under positive selection in species with unrooted molars based on the Bayes Empirical Bayes method for identifying sites under selection implemented in PAML (43). *Dspp* also had multiple sites with moderate support (posterior probability > 0.75). The overall selection patterns on each gene differed. Maximum likelihood estimates of selection for *Dspp* showed the percentage of sites under purifying and neutral selection on all branches were nearly equal (47% and 44%, respectively). Percentages of sites under positive selection in the species with unrooted molars (foreground branches) were nearly evenly divided as well, with 5% of sites from branches where the species with rooted molars (background branches) were undergoing purifying selection and 4% of sites from branches where the species with rooted molars were under neutral selection. For *Aqp1*, nearly all sites were under purifying selection on all branches (91%), and few sites were under neutral selection on all branches (7%). Few sites were undergoing positive selection in the foreground branches and their distribution also was unevenly split between sites under purifying and neutral selection on background branches (0.6% and 0.04%, respectively). The complete list of dental genes with hierarchical orthogroups, microsynteny clusters, and positive selection test results are available in Additional file 1.

Because genes under positive selection are often expressed at lower levels than genes under purifying selection (44–47), we also compared expression levels of *Dspp* and *Aqp1* in postnatal first molars (M1) at postnatal days 1, 15, and 21 (P1, P15, and P21) in bank voles (rooted molars) and prairie voles (unrooted molars) using quantitative PCR. Prairie vole molars expressed *Aqp1* at significantly lower levels in all three ages than bank vole molars (Fig. 3). Prairie vole P1 molars expressed significantly lower levels of *Dspp* than bank vole molars; at

P15 and P21, their molars expressed *Dspp* at lower, but not statistically significantly different, levels than their bank vole equivalent. For both genes, the prairie vole had consistent expression levels across three biological replicates, while the bank vole had greater variation in expression levels across replicates.

Sequence and secondary structure evolution

To detect whether substitutions at sites under positive selection influenced protein structure and evolution, we analyzed ancestral states and secondary structure across Glires. We first reconstructed ancestral sequences along the internal nodes of the Glires phylogeny for the genes undergoing branch-and-site specific positive selection to assess potential secondary structural changes in their protein sequences. At the best-supported site in *Dspp* (position 209 in the gapped alignment, Additional file 2), there were three major amino acid changes. The ancestral Glires sequence started with an asparagine (N) in this position. Two of the three species with unrooted molars represented in the *Dspp* dataset had amino acid substitutions at this position, with *Oryctolagus cuniculus* substituting a leucine (L) and *Dipodomys ordii* substituting an aspartic acid (D) at this position (Fig. 4A). All muroids (the clade including the voles in family Cricetidae and mice and rats in family Muridae) in our phylogeny substituted histidine (H) for the asparagine at this position. The secondary structure predicted at this position was a coil for most sequences but a helix for the *D. ordii* sequence (Fig. 5). *Aqp1* sequences varied greatly at the position under putative positive selection in species with unrooted molars (position 294 in the gapped alignment, Additional file 3). The ancestral state reconstruction showed twelve changes of the amino acid at this position across Glires (Fig. 4B), yet these changes did not

affect the predicted secondary structure of the protein near this residue, which was a coil for all sequences tested. All secondary structure predictions are available in Additional file 4.

Developmental gene expression

We also assessed differential gene expression between mouse and bank vole molars across early development to study the effects of morphology on expression levels of dental genes. Our gene expression analysis focused on keystone dental gene categories, which are based on the effects null mutations of each gene are reported to have during embryonic dental development (48): “shape” genes cause morphological errors, “eruption” genes prevent tooth eruption, “progression” genes stop the developmental sequence, “tissue” genes cause defects in tissues, “developmental process” genes are annotated with the “GO:0032502” gene ontology term, and “dispensable” genes, while dynamically expressed in developing teeth, have no documented effect on phenotype. The group “other” is composed of the remaining protein coding genes (48). Our bank vole genome was like the mouse and rat genomes in terms of the numbers and expression patterns of genes annotated from these keystone categories (Table 2). Ordination of gene expression results from the bank vole and mouse data at embryonic day 13, 14, and 16 (E13, E14, E16) (48) by principal components analysis showed a distinct separation between the mouse and bank vole along the first principal component (PC1) of the 500 most variable genes (Fig. 6A). PC1 explained 82.81% of the variance in these genes; there are distinct, species-specific expression patterns in these tissues. Along PC2 (7.47% of variance explained), E13 and E14 samples differ from the E16 samples, although the difference in time points is much greater in bank voles. Ordination of just the keystone dental genes showed clear separations between tissues based on species and age (Fig. 6B). Within this focused set of genes,

252 however, PC1 and PC2 explain less variance (44.8% and 28.84% respectively), and how species
253 and age relate to the PCs is less clear. There are two distinct, parallel trajectories for the mouse
254 and bank vole. Although within each species there is separation by age along PC1 and PC2,
255 mouse E16 and bank vole E13 occupy a similar position along PC1, and mouse E13 and bank
256 vole E16 occupy a similar position along PC2.

257 Examining individual genes underlying the differences between mouse and vole molars,
258 we note several upregulated genes in our vole molars are broadly expressed in developing molars
259 of other vole species (49,50). Relative to the mouse molars, vole molars overexpressed genes
260 related to forming tooth cusps, including *Bmp2*, *Shh*, *p21* (also known as *Cdkn1a*), and *Msx2*, a
261 difference explained by the faster patterning and larger number of cusps in the vole molar
262 compared to the mouse molar (50). Another gene upregulated in the patterning stage vole molar
263 is *Fgf10*, which is associated with delayed root formation later in vole molar development (9).

264 Nevertheless, developing bank vole molars at E13, E14, and E16 expressed keystone
265 dental genes in overall proportions like those observed at analogous stages of mouse and rat
266 molar development (Fig. 7). Permutation tests within each bank vole sample showed that log
267 counts for the set of genes related to the progression of dental development were significantly
268 higher than those in the tissue, dispensable, developmental process, and "other" categories at E14
269 and E16. The progression gene counts in E13 molars were higher for all of these except the
270 dispensable category. Shape category genes also were significantly higher than "other" category
271 genes in the E14 tissue. Overall, even though we observed conserved expression patterns of
272 dental genes at the system level, individual genes involved in cusp patterning and morphology
273 differed between the mouse and the vole.
274

DISCUSSION

Our two goals in sequencing the genome of *Myodes glareolus* were to support the development of a comparative system for studying tooth root development and to investigate the evolution of dental genes in Glires, a clade in which ever-growing molars have evolved multiple times (1). Our new *M. glareolus* assembly and annotation captured nearly all of the single-copy orthologs for Euarchontoglires and provided scaffolds with sufficient length for synteny analyses. It was well represented in ortholog groups and microsynteny clusters across Glires. We tested the hypothesis that dental genes are undergoing site-specific positive selection in species with unrooted molars (branch-and-site specific positive selection (42)) and exhibit differential expression patterns. We predicted that lack of conserved syntenic relationships in species with unrooted molars could place dental genes in regulatory and selective environments that promote changes among genes relevant to tooth root formation. Our analyses revealed that most dental genes have conserved syntenic relationships across Glires, yet two dental genes, *Dspp* and *Aqp1*, were undergoing positive selection in species with unrooted molars. We also demonstrated conserved patterns of gene expression among dental keystone genes between bank voles and mice during early embryonic development, and deviations from these conserved patterns likely related to differences in molar morphology between the two species.

We identified 13 genes which were not syntenic in at least half of the species with unrooted molars, and 6 genes undergoing site-specific positive selection across all Glires. Only one gene, *Col4a1*, lacked synteny and had evidence of positive selection. The two genes undergoing positive selection in species with unrooted molars, *Dspp* and *Aqp1*, both maintained their synteny relationships across the Glires studied. Although we predicted loss of synteny for dental genes in Glires with unrooted molars could result in sequence evolution by placing genes

298 in new selective contexts, our analyses did not support a relationship between non-syntenic genes
299 and positive selection. Maximum likelihood estimates of sites under different types of selection
300 for the genes with branch-specific positive selection did reveal different selective pressures on
301 *Dspp* and *Aqp1* overall; *Dspp* sites on background branches (i.e., branches with species that have
302 rooted molars) were under a mix of purifying and neutral selection, while nearly all *Aqp1*
303 background branch sites were under purifying selection. These selection regimes suggest there is
304 greater conservation for *Aqp1* function across Glires than for *Dspp* function. Gene duplication
305 can result in functional redundancy and evolution toward a novel function in some genes (51–
306 54), which may explain positive selection in *Aqp1*, as there are other aquaporin family genes
307 present. *Dspp* has no paralogs, but overlaps functionally with other SIBLING family proteins
308 (e.g., *Opn*, *Dmp1*) (55,56).

309 *Aqp1* and *Dspp* play different functional roles during dental development. Under the
310 keystone dental development gene framework, *Aqp1* is a "dispensable" gene: developing teeth
311 express it, but tooth phenotypes do not change in its absence. *Aqp1* is expressed in endothelia of
312 microvessels in the developing tooth (57,58). *Dspp* may be particularly relevant for the
313 formation of an unrooted phenotype if its expression domain or function have been modified in
314 species with unrooted molars. *Dspp* is a "tissue" category keystone dental gene, meaning the
315 main effects of a null mutation occur during the tissue differentiation stage of dental
316 development (48). Null mutations of *Dspp* cause dentin defects in a condition called
317 dentinogenesis imperfecta (59,60); in some patients, teeth form short, brittle roots (60,61). *Dspp*
318 knockout mice also exhibit the shortened root phenotype, among a variety of other defects in
319 both endochondral and intramembranous bone, due to the disruption of collagen and bone
320 mineralization (62–64).

Our ancestral sequence reconstructions and estimated secondary protein structures allowed us to assess whether nonsynonymous substitutions at sites under positive selection resulted in structural differences, thus potentially affecting protein function. Although unrooted molars are a convergent phenotype across Glires, the sites under positive selection did not converge on the same amino acid substitution in species with unrooted molars, and *Aqp1* appeared particularly labile at this residue. The non-synonymous substitutions at these sites often resulted in changes of properties of the amino acid in the sequence, for example in *Dspp*, polar asparagine was replaced with non-polar leucine in *O. cuniculus*. Only one of these substitutions changed the predicted secondary structure. Nevertheless, single amino acid substitutions do produce phenotypes for both *Dspp* (65) and *Aqp1* (66), thus we cannot rule out functional changes in these genes in species with unrooted molars.

Although the exact relationship between gene expression and sequence divergence remains unclear (67), studies of genome evolution across small numbers of mammal species show correlations between gene sequence divergence and levels of expression (68). In particular, highly-expressed genes are more likely to experience purifying selection (44–47), while lowly-expressed genes and tissue-specific genes may experience positive selection (45). The decreased expression of *Dspp* and *Aqp1* in prairie vole M1 compared to that of the bank vole M1 thus supports our finding of positive selection in these genes in species with unrooted molars. If all species with unrooted molars also exhibit decreased expression levels of *Dspp* and *Aqp1*, it could suggest a strong link between lower levels of the genes and the unrooted phenotype.

Without analyses of functional variation caused by positive selection at these coding sites, or spatial sampling to determine where these genes may be expressed during development, we are limited from exploring the specific effects of *Dspp* and *Aqp1* on root formation.

Nevertheless, we found evidence for evolution of these genes in Glires with unrooted molars, and *Dspp* especially has clinical relevance for tooth root formation. Future studies should explore the spatial distribution of *Dspp* expression, which could be relevant to functional changes in Glires with unrooted molars. If *Dspp* is relevant to the lack of root formation in hypselodont Glires incisors, the positive selection identified here may modify its expression domain or its interaction with yet-unidentified root formation co-factors, thus serially reproducing the unrooted incisor phenotype in molars.

Our RNA sequencing results supported the bank vole as a suitable system for studying dental development. Although molar morphology differs considerably across mammals, candidate-gene approaches have identified numerous conserved genes involved in tooth development and morphological patterning (69). Studies of single genes or gene families have identified shape-specifying roles common to multiple species (50,70–72), and high-throughput sequencing of mouse and rat molars demonstrate that both species express sets of dental development genes in similar proportions during early stages of tooth development (48). The similarity of our high-throughput RNA sequencing results to the mouse and rat results in previous studies suggest overall expression patterns of keystone dental development genes within each stage may be conserved in Glires. Our principal component analyses and differential expression analyses measuring changes between mouse and bank vole molars, however, showed that several dental genes' expression levels differed significantly by species and age. Previous research has documented organ expression patterns that are conserved across species early in development and diverge over time, with some major organs displaying heterochronic shifts in some species (73). If the major source of variation in keystone dental gene expression patterns between mice and bank vole molars were solely attributable to species, we might expect to see

clear separation between the species along the first or second principal component (PC1 or PC2), like that observed in PC1 of the 500 most variable genes (Fig. 6). If molar development follows the diverging expression patterns observed in other organs, we might expect just the earliest age classes to align on one, or multiple, PCs. Instead, we found two trajectories that were nearly parallel across PC1 and PC2 and multiple keystone dental genes that were significantly differentially expressed with respect to species and age. This variation between species is likely driven by the larger number of cusps in the vole molar, and corresponding upregulation of genes regulating cusp formation. The overall acceleration of patterning in vole molars likely explains the significance of the age variable in our expression results, causing a heterochronic shift in the expression patterns.

Our analyses were limited by the small number of rodent species with sufficiently annotated genomes to be included in synteny and positive selection analyses. This limitation left us with a small phylogeny for our ancestral state reconstructions, which thus did not encompass the full diversity of Glires tooth roots, and potentially weakened model-based genomic analyses. Although positive selection analyses using the Bayes Empirical Bayes criterion are robust to smaller sample sizes (43), including fossil species in ancestral state reconstructions can change estimations of ancestral characteristics (74). Innovations in paleoproteomics also offer the opportunity to compare fossil species' dental gene sequences directly to living and estimated ancestral sequences (75,76). By incorporating data for extinct Glires in both morphological and molecular analyses, we can further elucidate links between dental gene evolution and unrooted teeth.

CONCLUSIONS

Our genomics and transcriptomics analyses, based on our newly sequenced, high-quality draft bank vole genome assembly and annotation, showed that bank vole early tooth development is comparable to other commonly used rodent models in dental development research. We identified 6 dental gene orthogroups that were undergoing site-specific positive selection across Glires and two genes, *Dspp* and *Aqp1*, that were undergoing site-specific positive selection in Glires with unrooted molars. *Dspp* appears particularly relevant to root formation, as loss-of-function mutations cause a dentin production defect that can result in shortened tooth roots. Future research must explore the functional role that *Dspp* plays in tooth root formation in Glires and other clades. The rodent dentary is an exciting system for understanding tooth development; it provides an easily manipulated set of tissues that can be produced quickly and features a lifelong population of stem cells in the incisor with genomic mechanisms that are potentially replicated across other teeth in species with unrooted molars. Our results identify candidate genes for future analyses, and our draft bank vole genome and annotation improve the utility of this species for comparative dental research that can uncover the genetic mechanisms of tooth root formation.

METHODS

Tissue collection and sequencing

To assemble the bank vole genome, we sequenced tissues from a single adult male specimen housed in a colony at the UCSF Mission Center Animal Facility. We euthanized the animal according to UCSF IACUC protocol AN189916 and harvested muscle, kidney, heart, and liver tissue, which were immediately frozen at -80°C. Tissues were sent to a third-party sequencing service, where they were combined and homogenized to achieve appropriate mass

for high molecular weight DNA extraction. We targeted 60x coverage with 150 base pair (bp) reads using 10X Chromium linked-read chemistry (77,78) and sequenced on the Illumina platform. We also targeted 10x coverage with Pacific Biosciences SMRT long-read chemistry. For genome annotation and gene expression analyses, we collected seven biological replicates each of first molars at embryonic days 13-16 (E13, E14, E15, E16), second molars at E16, and jaw tissues at E14 under University of Helsinki protocols KEK16-021, KEK19-019, and KEK17-030 and stored them in RNAlater at -80°C for RNA sequencing, following a tissue harvesting protocol established for mice and rats (48). We extracted RNA from these tissues using a guanidium thiocyanate and phenol-chloroform protocol combined with an RNeasy column purification kit (Qiagen) based on the keystone dental gene protocol (48). Single-end 84 bp RNA sequencing was performed using the Illumina NextSeq 500 platform.

Genome assembly and quality control

We first assembled only the 10X Chromium linked reads using the default settings in Supernova 2.1.1. (77,78). We selected the "pseudohaplotype" (pseudohap) output format, which randomly selects between potential alleles when there are two possible contigs assembled for the same region. This option produces two assemblies, each with a single resolved length of the genome sequence (77–79). We used our lower-coverage, long-read data for gap filling and additional scaffolding. First, we estimated the genome's length using the raw sequence data in GenomeScope (80), which predicted a length of 2.6 gigabases. We then performed error correction of the long reads using Canu (81), removing reads shorter than 500 bp and disregarding overlaps between reads of fewer than 350 bp. We kept only those reads with minimum coverage of 3x for scaffolding. Following long read error correction, we used Cobbler

and RAILS (82) with a minimum alignment length of 200 bases to accept matches for gap filling and scaffolding of both pseudohap assemblies.

For quality control, we assessed both unscaffolded and long-read scaffolded pseudohap assemblies by standard assembly length statistics with QUAST (83) and presence of single-copy orthologs with BUSCO v3 (84). Both scaffolded assemblies were approximately 2.44 Gigabases long, with an N50 (the length of the shortest scaffold at 50% of the total assembly length) of 4.6 Megabases; we refer to them as Pseudohap1+LR and Pseudohap2+LR. The Pseudohap1+LR assembly had 17,528 scaffolds over 1000bp (base pairs) long, and the Pseudohap2+LR assembly had 17,518 scaffolds over 1000bp long (Table 3). BUSCO searched for universal single-copy orthologs shared by Euarchontoglires, recovering 89.4% of these genes in the scaffolded Pseudohap1+LR assembly and 92.8% of the single-copy orthologs in the scaffolded Pseudohap2+LR assembly (Fig. 8). The two assemblies were similar length and contiguity, but because the scaffolded Pseudohap2+LR assembly recovered more single-copy orthologs, we based annotation and downstream analyses on it.

Genome annotation

We annotated the genome using three rounds of the MAKER pipeline (85–87). MAKER combines multiple lines of evidence to annotate a genome. For evidence from gene transcripts, we assembled a *de novo* transcriptome assembly based on the single-end RNA sequencing of all molar and jaw tissues using Trinity (88). We also included cDNA sequences from the *Mus musculus* assembly GRCm38. We used SwissProt's curated protein database to identify protein homology in the genome. Two libraries of repeats provided information for repeat masking: the Dfam Rodentia repeat library (89–91) and a custom library specific to the bank vole estimated

based on the modified protocol of Campbell et al. (86). The custom library features miniature inverted-repeat transposable elements identified with default settings in MiteFinder (92), long terminal repeat retrotransposons extracted with the GenomeTools LTRharvest and LTRdigest functions (93) based on the eukaryotic genomic tRNA database, and *de novo* repeats identified with RepeatModeler (94). We combined elements identified by these programs into a single repeat library, then removed any elements that matched to a custom SwissProt curated protein database with known transposons excluded; this custom repeat library is available in Additional file 5. We trained a custom gene prediction model for MAKER as well. The first iteration of the model came from BUSCO's implementation of augustus (95). Between each round of MAKER annotation, we updated the gene prediction model with augustus.

MAKER considered only contigs between 10,000-300,000 bp long during annotation. Our second and third iterations of MAKER used the same settings but excluded the "Est2genome" and "protein2genome" functions, as recommended in the MAKER tutorial. We included a SNAP (96) gene prediction model based on the output of the first round of annotation during the second and third iterations of MAKER annotation. Annotation quality (i.e., agreement between different lines of evidence and the MAKER annotation) was assessed visually in JBrowse after each iteration and using *compare_annotations_3.2.pl* (97), which calculates the number of coding and non-coding sequences in the annotation in addition to basic statistics about sequence lengths. Our MAKER annotation covered 2.41 Gb of the scaffolded Pseudohap2 assembly in 4,125 scaffolds. These scaffolds contained 27,824 coding genes (mRNA) and 15,320 non-coding RNA sequences. The average gene length was 12,705 bp. Most annotations (91.4%) had an annotation edit distance (AED) of 0.5 or better. AED is a measure of congruency between

481 the different types of evidence for an annotation, where scores closer to zero represent better-
482 annotated genes (98).
483
484 *Orthology and synteny analyses*
485 We analyzed orthology and synteny of the bank vole genome to understand gene and
486 genome evolution related to dental development across Glires with rooted and unrooted molars.
487 We obtained genomes from Ensembl for 23 Glires species and one phylogenetic outgoup, *Homo*
488 *sapiens* (Table 4). These genomes all had an N50 over 1 Mb, which improves synteny
489 assessment (99). We first analyzed all 24 genomes for groups of orthologous genes (orthogroups)
490 in OrthoFinder (100), providing a tree topology based on the Ensembl reference tree (Fig. 1) to
491 guide orthology detection. Because we would not analyze the human outgroup in downstream
492 analyses, we implemented the OrthoFinder option that splits orthogroups at the root of Glires
493 (hierarchical orthogroups), thus any group of orthologs studied here represents only genes with
494 shared, orthologous evolutionary history within Glires. We selected MAFFT (101) for multiple
495 sequence alignment and fastme (102) for phylogenetic tree searches within OrthoFinder; we
496 retained the gene trees estimated for each orthogroup for downstream analyses.
497 Although dental development genes are spread throughout the genome, we were
498 interested in whether each gene remained in the same local arrangement across species of Glires.
499 We prepared each genome annotation and sequence file for synteny analysis using the
500 reformatting functions of Synima (103) to extract each peptide sequence associated with a gene
501 coding sequence in the Ensembl annotation. Collinear synteny blocks estimated by MCScanX
502 (104) formed the basis for microsynteny network analyses using the SynNet pipeline (105–107).
503 We inferred networks from the top five hits for each gene, requiring any network to have a

minimum of 5 collinear genes and no more than 15 genes between a collinear block, settings that perform well for analyzing mammal genomes (107). Using the infomap algorithm, we clustered the synteny blocks into microsynteny networks, from which we extracted network clusters corresponding to the list of keystone dental genes (48). For each dental gene microsynteny network, we assessed whether genes of species with unrooted molars were not syntenic with the other Glires species' sequences.

Positive selection analysis

We aligned protein sequences for each dental gene orthogroup with clustal omega (108) using default settings. Based on universal translation tables, we obtained codon-based nucleotide alignments with pal2nal (109), removing sites in which any species had an indel (i.e., ungapped) and formatting the output for analysis in PAML (41). We pruned and unrooted the orthogroup gene trees from OrthoFinder to contain only tips representing the genes in each synteny network or orthogroup under analysis in PAML. We tested whether any of the genes were undergoing positive selection using a likelihood ratio test comparing site-specific models of "nearly neutral" and positive selection. In these models, ω, the ratio of nonsynonymous to synonymous nucleotide substitutions (also known as dN/dS), can vary at each codon site. In the "nearly neutral" model, ω can take values between 0 and 1, while the positive selection model allows sites to assume ω values greater than 1 (43,110). We allowed PAML to estimate κ (the ratio of transitions to transversions) and ω from initial values of 1 and 0.5, respectively, for both tests.

Dental genes with significant site-specific positive selection or those for which over half the unrooted species' sequences were not in the same synteny block as sequences for species with rooted molars formed the basis for our second set of positive selection tests using a branch-

and-site model of positive selection. This model allows ω to vary not only among codon sites, but also between "foreground" and "background" lineages (43). We marked the species with unrooted molars as foreground lineages, then ran the model twice: once with ω unconstrained to detect sites undergoing positive selection only on foreground branches, and a second time and with ω fixed to 1, or neutral selection. A likelihood ratio test of the two models determined whether the lineage-specific positive selection model was more likely than a neutral model, and Bayes Empirical Bayes analyses (43) produced posterior probabilities to identify sites under positive selection.

Genes under positive selection also tend to have lower expression levels (45), thus we compared expression of the genes with branch-and-site specific positive selection between the prairie (unrooted molars) and the bank vole (rooted molars) to provide further support for selective differences. We collected three biological replicates of first molars from both species at three postnatal stages (P1, P15, and P21) and immediately preserved them at -80°C in lysis buffer (Buffer RLT; Qiagen) supplemented with 40 µM dithiothreitol. RNA was extracted from homogenized tissues using a RNeasy column purification kit (Qiagen). We assessed concentration and purity of extracted RNA using a NanoDrop 2000 spectrophotometer (ThermoFisher Scientific). Using 1 µg of RNA, we synthesized cDNA using a high-capacity cDNA reverse transcription kit (ThermoFisher Scientific). We used 1 µL diluted cDNA (1:3 in ddH_2O) and iTaq Universal SYBR Green Supermix (Bio-rad) in the Bio-rad CFX96 real-time PCR detection system for qPCR experiments, producing three technical replicates for each biological replicate. We normalized cycle threshold (CT) values of genes of interest to GAPDH expression levels and calculated relative expression levels as $2^{-\Delta\Delta CT}$. A two-tailed unpaired t-test calculated in Prism 9 measured whether expression of these genes significantly differed between

bank voles and prairie voles. The oligonucleotide primers for each species and gene are in Additional file 6.

Sequence and secondary structure evolution

We performed ancestral sequence reconstruction on the codon sequences of the genes that had evidence of branch-and-site specific positive selection to understand how the sequence has changed through time. The gapped clustal omega alignments were the basis for ancestral sequence reconstruction on the Glires species tree (Fig. 1) using pagan2 (111). For each gene, we plotted amino acid substitutions at the site with potential positive selection. Finally, we predicted secondary structures (i.e., helices, beta sheets, and coils) for each unrooted species' protein sequence and the reconstructed ancestral sequence prior to the change at the site under positive selection using the PSIPRED 4.0 protein analysis workbench (112,113). Comparing these predictions across the phylogeny, we assessed how these substitutions at the site under selection may affect the structure of each protein.

Developmental gene expression

We used performed quality control and filtering of the short reads for the seven replicates of first molar tissues at E13, E14, and E16 using the nf-core/rnaseq v. 3.11.2 workflow (114) for comparability to previous mouse and rat analyses (48). RNAseq reads were evaluated and adapter sequences were filtered using FastQC v. 0.11.9 (115) and Cutadapt v. 3.4 (116), and ribosomal RNA was removed using SortMeRNA v. 4.3.4 (117). We then aligned trimmed sequences to our bank vole annotation using Salmon v. 1.10.1 (118). Counts were then normalized by gene length. We categorized gene count data into functional groups based on their

established roles in tooth bud development (48) using the one-to-one orthology list between our bank vole genome and the mouse GRCm39.103 genome annotation generated from our OrthoFinder output. Using the rlog function of DESeq2 (119), we normalized gene counts within each functional group on a log2 scale. A permutation test assessed whether the mean counts of the progression, shape, and double functional groups were significantly different from genes in the tissue, dispensable, and "other" groups (which are potentially relevant later in development) based on 10,000 resampling replicates of the dataset (48).

We also assessed differential expression between the bank vole first molar and published mouse M1 data at the same three time points (GEO accession GSE142199 (48)), combining the data based on the one-to-one orthology relationships used in the functional permutation analysis. Using the mouse E13 molar as the reference level, we modeled expression as a response to species (mouse or vole), embryonic day (E13, E14, or E16), and the interaction between species and day. We considered as significant any gene with a log fold change greater than 1, log fold change standard error less than 0.5, and false discovery rate adjusted p value less than 0.05.

596 TABLES

597 **Table 1 – Genes undergoing site-specific and branch-and-site-specific positive selection**

Gene	*Mus* transcript	*Myodes* transcript	Site	Branch-and-site
Aqp1	ENSMUST00000004774	Mglareolus_00011822	Yes	Yes
Col4a1	ENSMUST00000033898	Mglareolus_00032740	Yes	No
Dspp	ENSMUST00000112771	Mglareolus_00014030	Yes	Yes
Fgf20	ENSMUST00000034014	Mglareolus_00013079	Yes	No
Runx3	ENSMUST00000056977	Mglareolus_00033992	Yes	No
similar to *Runx3*	–	–	Yes	No*

598 Table 1 Legend: *HOG only contained four genes with one unrooted species' sequence, could

599 not be tested for branch-and-site specific selection.

600

601 **Table 2 – P-values of permutation tests between keystone gene categories in bank vole M1**

602 **at embryonic days 13, 14, and 16**

		Tissue	Dispensable	Dev. Process	Other
E13	**Progression**	*0.0310*	0.0942	*0.0436*	*0.0402*
	Shape	0.6431	0.9041	0.2289	0.0995
	Double	0.1292	0.1521	0.0716	0.0655
E14	**Progression**	*0.0136*	*0.0383*	*0.0437*	*0.0401*
	Shape	0.3115	0.4725	0.0922	*0.0454*
	Double	0.1288	0.0945	0.0709	0.0630
E16	**Progression**	*0.0140*	*0.0401*	*0.0303*	*0.0274*
	Shape	0.3770	1	0.1831	0.0662
	Double	0.1343	0.1099	0.0638	0.0596

603 Table 2 Legend: Italicized values are statistically significant ($p < 0.05$)

Table 3 – QUAST assembly statistics for *de novo* bank vole (*Myodes glareolus*) genome assemblies

	Pseudohap1	Pseudohap1+LR	Pseudohap2	Pseudohap2+LR*
Largest contig	27939478	32658832	27937749	32657565
Total length	2434151515	2441426554	2434099357	2441472313
GC (%)	41.88	41.89	41.88	41.89
N50	4187179	4579815	4187179	4558134
N75	1689669	1818134	1687188	1810460
L50	170	153	170	154
L75	388	357	388	358
Ns per 100 kbp	1151.99	1030.75	1151.96	1030.48

Table 3 Legend: *assembly used for annotation and downstream analyses in this paper.

Table 4 – Genomes used in orthology, synteny, and positive selection analyses

Species	Assembly	Citation
Myodes glareolus	CUNY_Mgla_1.0	This paper
*Cavia porcellus**	Cavpor3.0	(120)
*Cavia aperea**	CavAp1.0	(121)
Marmota marmota	marMar2.1	(122)
*Microtus ochrogaster**	MicOch1.0	(123)
Mus musculus	GRCm39	(124)
*Oryctolagus cuniculus**	OryCun2.0	(120)
*Dipodomys ordii**	Dord_2.0	(120)
Jaculus jaculus	JacJac1.0	(125)

Rattus norvegicus	Rnor_6.0	(126)
Mus pahari	PAHARI_EIJ_v1.1	(127)
Mus caroli	CAROLI_EIJ_v1.1	(127)
Mus spretus	SPRET_EiJ_v1	(128)
Mus spicilegus	MUSP714	(129)
Cricetulus griseus	CHOK1GS	(130)
Mesocricetus auratus	MesAur1.0	(131)
Peromyscus maniculatus	HU_Pman_2.1	(132)
Nannospalax galili	S.galili_v1.0	(133)
*Octodon degus**	OctDeg1.0	(134)
Heterocephalus glaber (F)	HetGla_female_1.0	(135)
*Chinchilla lanigera**	ChiLan1.0	(136)
Urocitellus parryi	ASM342692v1	(137)
Ictidomys tridecemlineatus	SpeTri2.0	(138)
*Homo sapiens***	GRCh38	(139)

609 Table 4 Legend: *Species with unrooted molars; **Peptide annotation used as outgroup only in
610 OrthoFinder analysis.
611
612
613
614
615
616

617 FIGURES

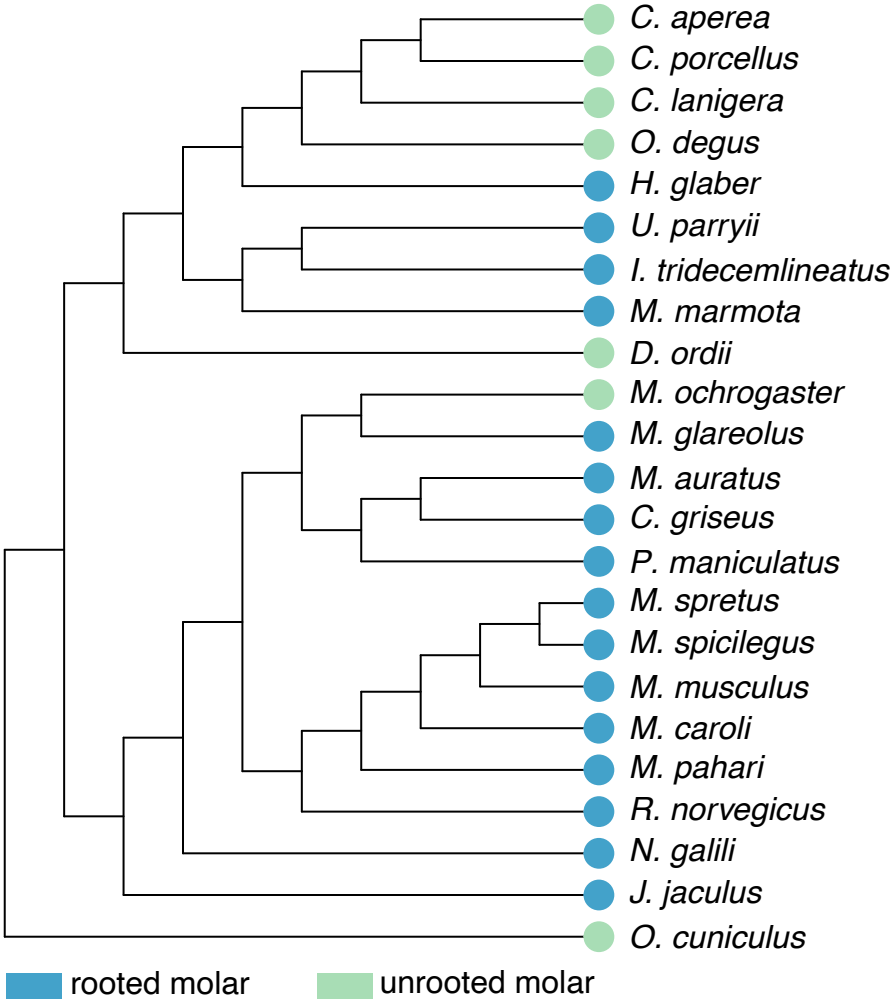

618

619 **Figure 1 –** Species tree of Glires based on the Ensembl Compara species tree. Whether each

620 species has rooted or unrooted molars is indicated at the tip of each branch. Note that unrooted,

621 or hypselodont, molars have evolved multiple times across Glires. This topology was the basis

622 for our orthology analysis.

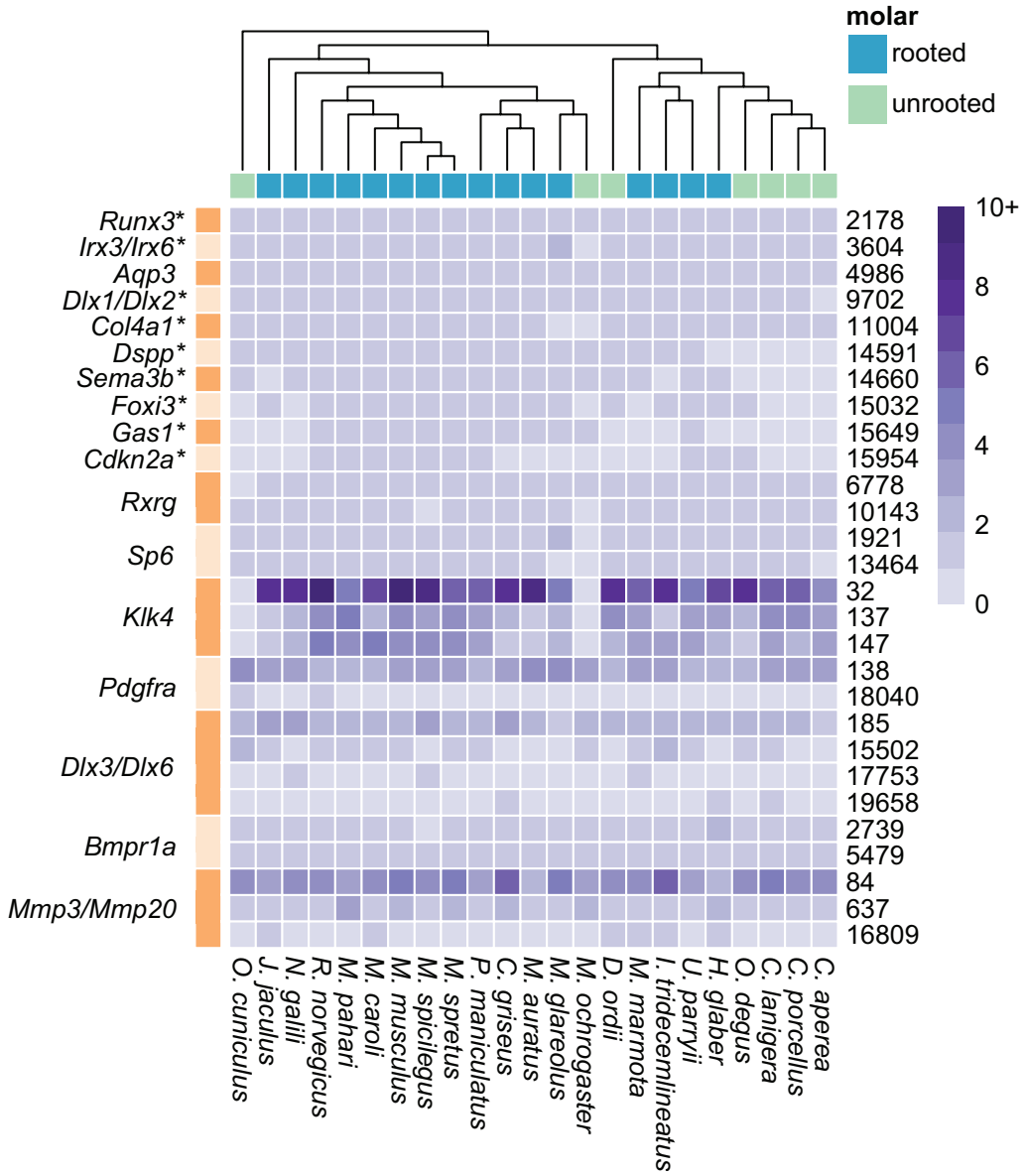

Figure 2 – Heatmap showing the number of genes per species (inset gradient scale from 0 to 10+) in each synteny cluster. The figure shows clusters where species with unrooted molars had no representation or did not have sequences in all microsynteny clusters associated with a single gene, clusters where more than one gene mapped to the same cluster, or a single gene mapped to multiple clusters. Microsynteny cluster number is noted on the right side of the heatmap (one row per cluster), and corresponding genes are noted on the left with alternating bands showing rows to which those genes mapped. * = genes where hierarchical orthogroup did not contain

646 genes for all 23 species. We found little evidence that non-syntenic genes in species with
647 unrooted molars are undergoing selection for novel functions.
648
649
650
651
652
653
654

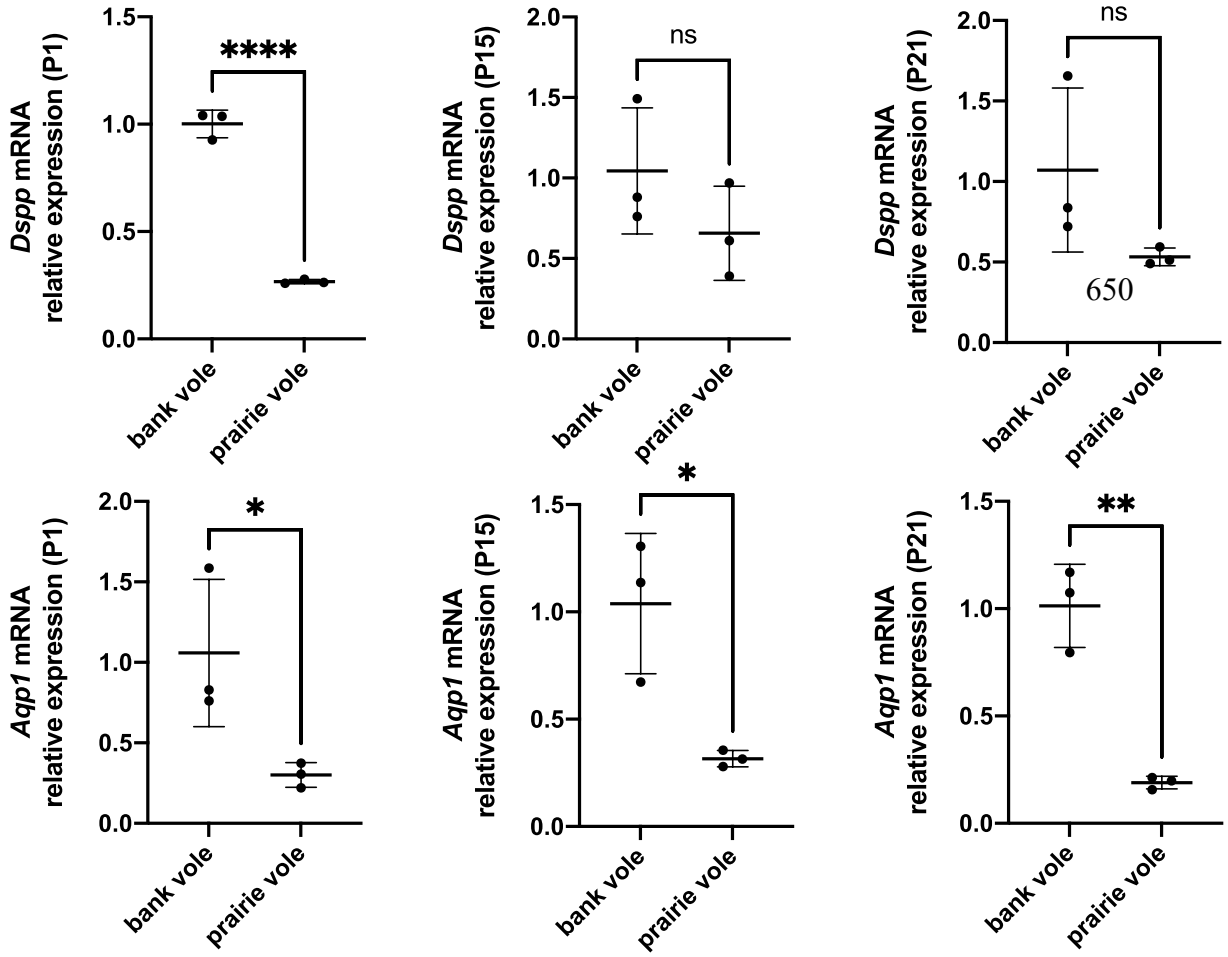

655 **Figure 3** – Quantitative PCR comparisons of *Dspp* and *Aqp1* expression between bank vole and
656 prairie vole M1 at postnatal days 1, 15, and 21 (P1, P15, P21). Expression levels for both genes
657 are lower in the prairie vole (unrooted molars), which supports the positive selection detected for
658 these genes in species with unrooted molars.
659
660

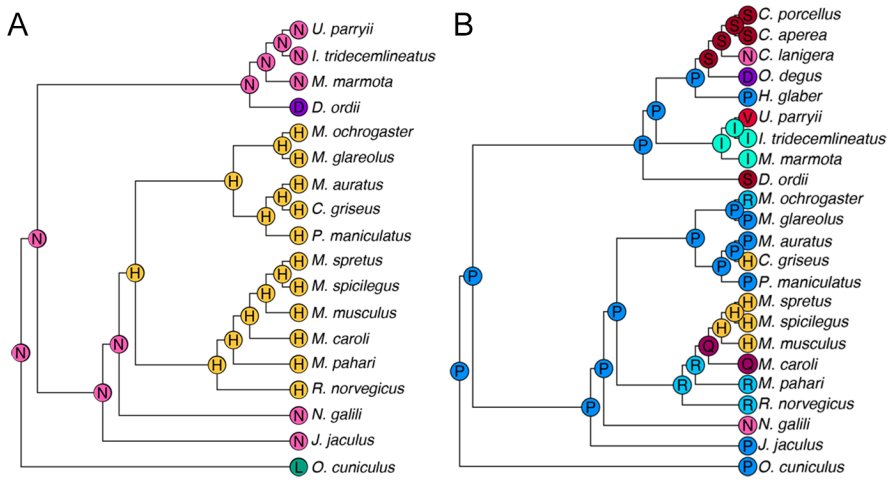

668 **Figure 4** – Ancestral state reconstructions of the residue under positive selection in PAML tests.

669 Letters at tips and internal nodes represent IUPAC codes for amino acids. **A** *Dspp*; **B** *Aqp1*.

670

671

672

673

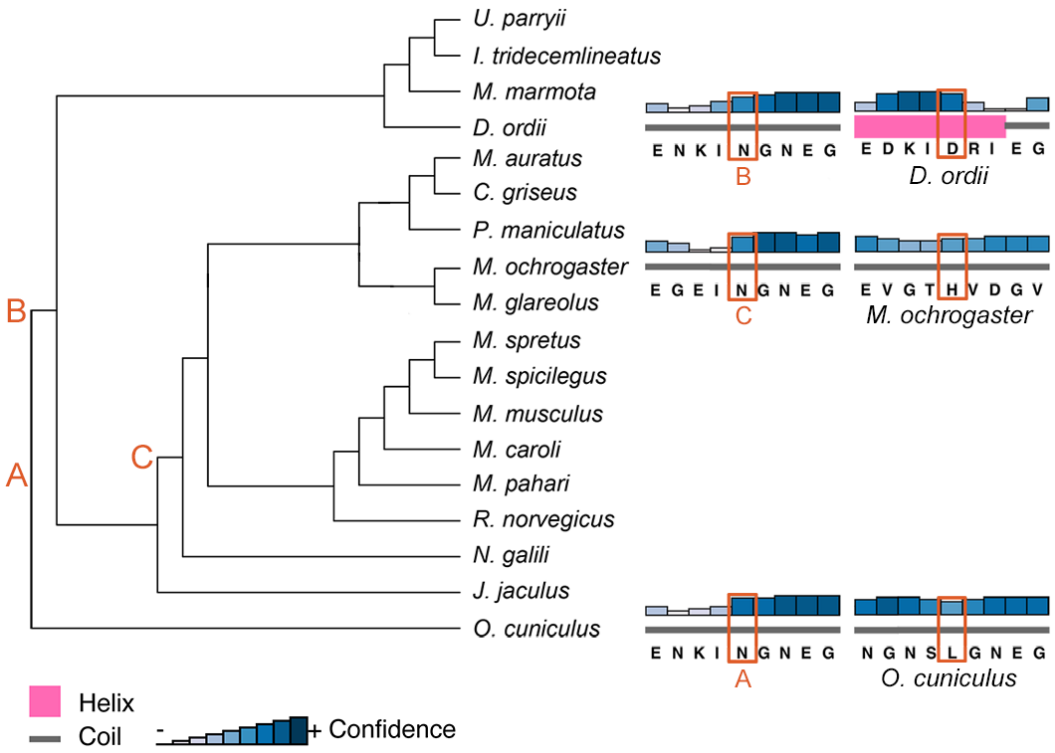

674

675 **Figure 5** – PSIPRED secondary structure predictions for the three species with unrooted molars

676 represented in the *Dspp* sequences. Letters correspond to the most recent ancestor of each tip

677 species that had a different amino acid at the position under positive selection.

678

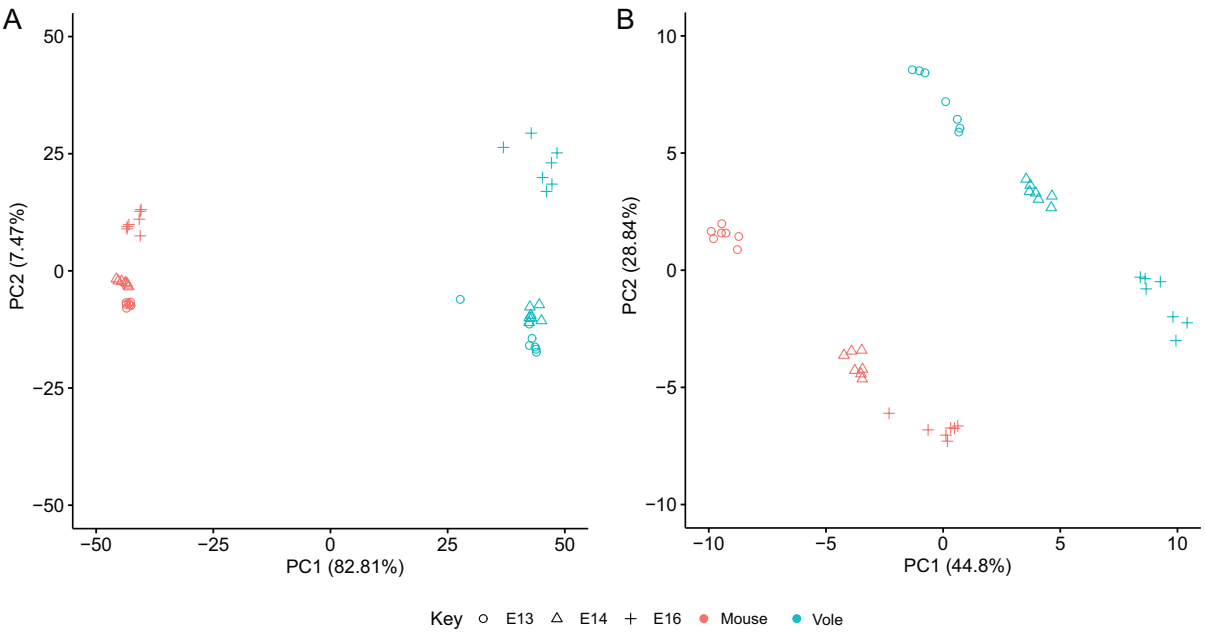

679

680 **Figure 6** – Principal component (PC) analyses of differentially expressed genes in mouse and
681 bank vole M1. **A** PC1 and PC2 of the 500 most variable genes, showing a clear differentiation
682 between species along PC1 and differentiation between age classes along PC2. **B** PC1 and PC2
683 of the keystone dental genes. Both PC1 and PC2 separate age classes within, but not between,
684 the species, likely due to differences in developmental timing and molar morphology between
685 mice and voles.

686

687

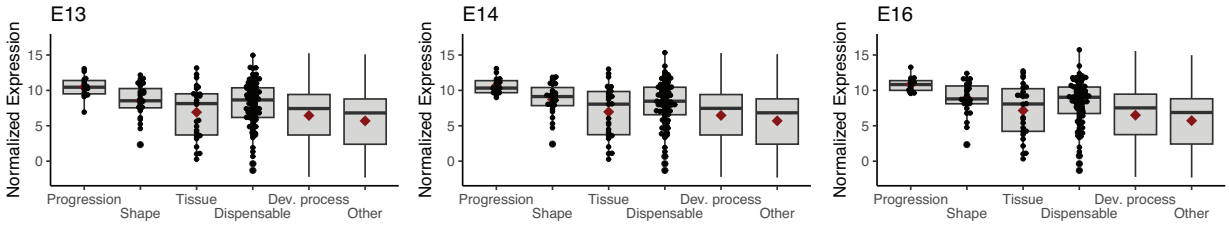

688 **Figure 7** – Box and whisker plots showing normalized log base 2 expression levels for each
689 keystone gene category in bank vole M1 at embryonic days 13, 14, and 16. Gene expression

690 profiles at these stages are comparable to mouse and rat molars at analogous developmental
691 stages, as seen in Hallikas et al. 2021.
692

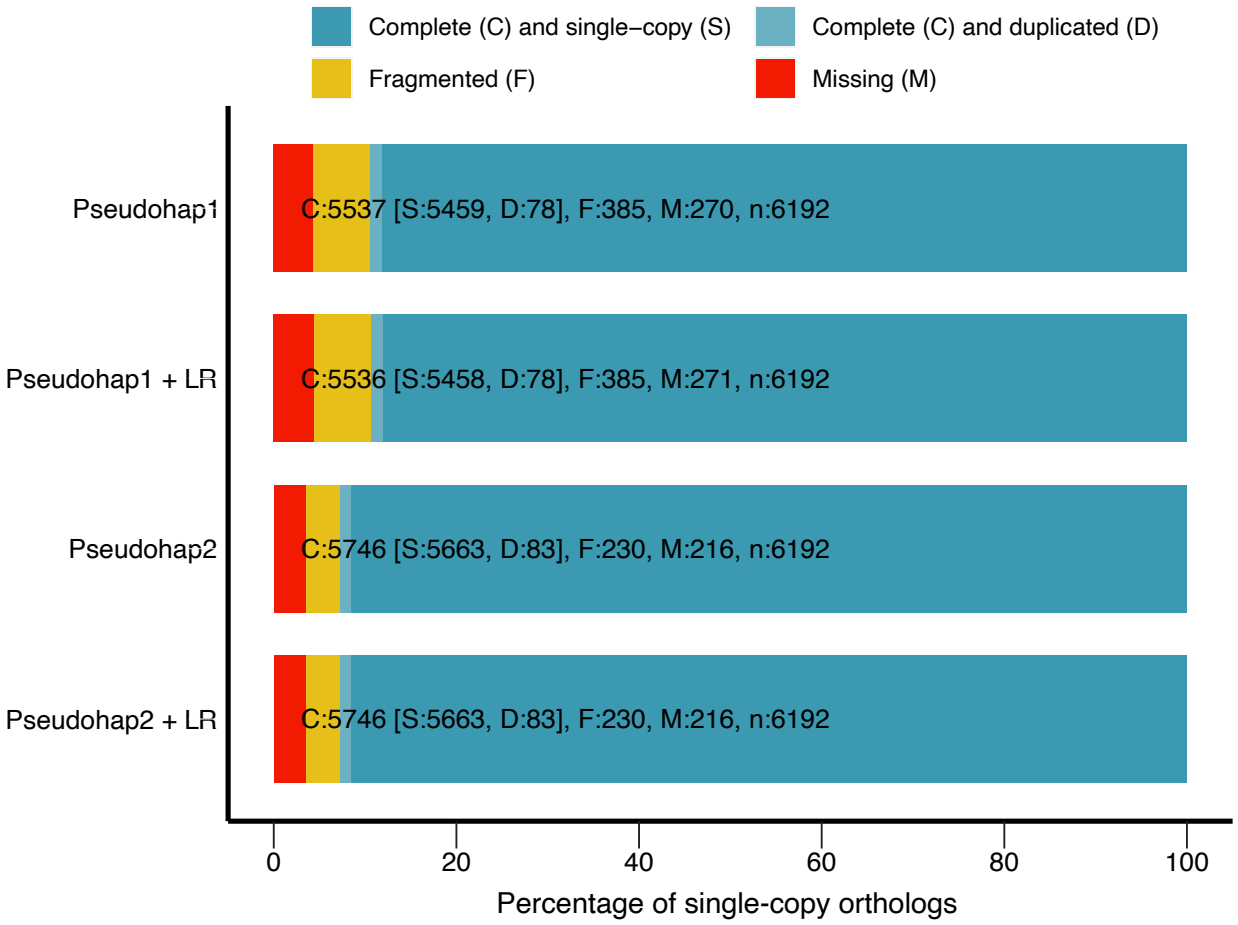

693

694 **Figure 8** – BUSCO single-copy ortholog recovery for each "pseudohaploid" version of our draft
695 bank vole genome assembly and these version after long-read scaffolding (denoted by "+ LR").
696 Each bar represents the cumulative proportion of the 6,192 single-copy orthologs for
697 Euarchontoglires identified by BUSCO represented by complete single-copy, complete-
698 duplicated, fragmented, and missing orthologs. The Pseudohap2 and Pseudohap2 + LR
699 assemblies had the best single-copy ortholog recovery.
700

ADDITIONAL FILES

Additional file 1 [.xlsx] Dental gene results – Full table of orthology, synteny, and positive selection test results for all dental genes assessed.

Additional file 2 [.txt] *Dspp* gapped alignment – Gapped codon-based alignment for *Dspp* in fasta formatted sequences.

Additional file 3 [.txt] *Aqp1* gapped alignment – Gapped codon-based alignment for *Aqp1* in fasta formatted sequences.

Additional file 4 [.pdf] Structure predictions – PSIPRED Secondary structure predictions for each ancestral node and unrooted molar tip species for *Dspp* and *Aqp1*.

Additional file 5 [.txt] Custom repeat library – Custom repeat library of fasta formatted sequences used in annotation of the draft *Myodes glareolus* genome. See Methods for description of the process used to generate the library.

Additional file 6 [.pdf] Oligonucleotide primers – List of oligonucleotide primers for *Dspp*, *Aqp1*, and *GAPDH* used in bank vole and prairie vole qPCR experiments.

REFERENCES

1. Renvoisé E, Michon F. An Evo-Devo perspective on ever-growing teeth in mammals and dental stem cell maintenance. Front Physiol. 2014;5 AUG(August):1–12.

2. Tapaltsyan V, Eronen JT, Lawing AM, Sharir A, Janis C, Jernvall J, et al. Continuously growing rodent molars result from a predictable quantitative evolutionary change over 50 million years. Cell Rep. 2015;11(5):673–80.

3. LeBlanc ARH, Brink KS, Whitney MR, Abdala F, Reisz RR. Dental ontogeny in extinct synapsids reveals a complex evolutionary history of the mammalian tooth attachment system. Proc R Soc B Biol Sci. 2018 Nov 7;285(1890):20181792.

4. Saffar JL, Lasfargues JJ, Cherruau M. Alveolar bone and the alveolar process: the socket that is never stable. Periodontol 2000. 1997;13(1):76–90.

5. Davit-Béal T, Tucker AS, Sire JY. Loss of teeth and enamel in tetrapods: Fossil record, genetic data and morphological adaptations. J Anat. 2009;214(4):477–501.

6. Damuth J, Janis CM. On the relationship between hypsodonty and feeding ecology in ungulate mammals, and its utility in palaeoecology. Biol Rev. 2011;86(3):733–58.

7. Miletich I, Sharpe PT. Normal and abnormal dental development. Hum Mol Genet. 2003 Apr 2;12(suppl_1):R69–73.

8. Harada H, Kettunen P, Jung HS, Mustonen T, Wang YA, Thesleff I. Localization of putative stem cells in dental epithelium and their association with Notch and FGF signaling. J Cell Biol. 1999;147(1):105–20.

9. Tummers M, Thesleff I. Root or crown: A developmental choice orchestrated by the differential regulation of the epithelial stem cell niche in the tooth of two rodent species. Development. 2003;130(6):1049–57.

10. Thesleff I, Tummers M. Tooth organogenesis and regeneration. In: StemBook. Cambridge, MA: Harvard Stem Cell Institute; 2008.

741 11. Krivanek J, Buchtova M, Fried K, Adameyko I. Plasticity of dental cell types in
742 development, regeneration, and evolution. J Dent Res. 2023 Jun 1;102(6):589–98.

743 12. Luan X, Ito Y, Diekwisch TGH. Evolution and development of Hertwig's epithelial root
744 sheath. Dev Dyn. 2006;235(5):1167–80.

745 13. Kumakami-Sakano M, Otsu K, Fujiwara N, Harada H. Regulatory mechanisms of Hertwig's
746 epithelial root sheath formation and anomaly correlated with root length. Exp Cell Res.
747 2014;325(2):78–82.

748 14. Wen Q, Jing J, Han X, Feng J, Yuan Y, Ma Y, et al. *Runx2* regulates mouse tooth root
749 development via activation of WNT inhibitor *NOTUM*. J Bone Miner Res.
750 2020;35(11):2252–64.

751 15. Yang S, Choi H, Kim TH, Jeong JK, Liu Y, Harada H, et al. Cell dynamics in Hertwig's
752 epithelial root sheath are regulated by β-catenin activity during tooth root development. J
753 Cell Physiol. 2021;236(7):5387–98.

754 16. Yamashiro T, Tummers M, Thesleff I. Expression of bone morphogenetic proteins and Msx
755 genes during root formation. J Dent Res. 2003;82(3):172–6.

756 17. Yokohama-Tamaki T, Ohshima H, Fujiwara N, Takada Y, Ichimori Y, Wakisaka S, et al.
757 Cessation of Fgf10 signaling, resulting in a defective dental epithelial stem cell
758 compartment, leads to the transition from crown to root formation. Development.
759 2006;133(7):1359–66.

760 18. Ota MS, Vivatbutsin P, Nakahara T, Eto K. Tooth root development and the cell-based
761 regenerative therapy. J Oral Tissue Eng. 2007;4(3):137–42.

762 19. Jernvall J, Thesleff I. Reiterative signaling and patterning during mammalian tooth
763 morphogenesis. Mech Dev. 2000;92:19–29.

764 20. Harada H, Toyono T, Toyoshima K, Yamasaki M, Itoh N, Kato S, et al. FGF10 maintains
765 stem cell compartment in developing mouse incisors. Dev Camb Engl. 2002;129(6):1533–
766 41.

767 21. Tapaltsyan V, Charles C, Hu J, Mindell D, Ahituv N, Wilson GM, et al. Identification of
768 novel *Fgf* enhancers and their role in dental evolution. Evol Dev. 2016;18(1):31–40.

769 22. Christensen MM, Hallikas O, Das Roy R, Väänänen V, Stenberg OE, Häkkinen TJ, et al.
770 The developmental basis for scaling of mammalian tooth size. Proc Natl Acad Sci. 2023
771 Jun 20;120(25):e2300374120.

772 23. Chen ZJ. Genetic and epigenetic mechanisms for gene expression and phenotypic variation
773 in plant polyploids. Annu Rev Plant Biol. 2007;58(1):377–406.

774 24. Stranger BE, Forrest MS, Dunning M, Ingle CE, Beazley C, Thorne N, et al. Relative impact
775 of nucleotide and copy number variation on gene expression phenotypes. Science. 2007 Feb
776 9;315(5813):848–53.

777 25. Romero IG, Ruvinsky I, Gilad Y. Comparative studies of gene expression and the evolution
778 of gene regulation. Nat Rev Genet. 2012 Jul;13(7):505–16.

779 26. de Montaigu A, Giakountis A, Rubin M, Tóth R, Cremer F, Sokolova V, et al. Natural
780 diversity in daily rhythms of gene expression contributes to phenotypic variation. Proc Natl
781 Acad Sci. 2015 Jan 20;112(3):905–10.

782 27. Erwin DH, Davidson EH. The last common bilaterian ancestor. Development. 2002 Jul
783 1;129(13):3021–32.

784 28. Irie N, Kuratani S. Comparative transcriptome analysis reveals vertebrate phylotypic period
785 during organogenesis. Nat Commun. 2011;2:248.

786 29. Koonin EV. Evolution of genome architecture. Int J Biochem Cell Biol. 2009 Feb
787 1;41(2):298–306.

788 30. Wray GA. The evolutionary significance of cis-regulatory mutations. Nat Rev Genet. 2007
789 Mar;8(3):206–16.

790 31. Acemel RD, Maeso I, Gómez-Skarmeta JL. Topologically associated domains: A successful
791 scaffold for the evolution of gene regulation in animals. WIREs Dev Biol. 2017;6(3):e265.

792 32. Coghlan A, Eichler EE, Oliver SG, Paterson AH, Stein L. Chromosome evolution in
793 eukaryotes: A multi-kingdom perspective. Trends Genet. 2005 Dec 1;21(12):673–82.

794 33. Swenson KM, Blanchette M. Large-scale mammalian genome rearrangements coincide with
795 chromatin interactions. Bioinformatics. 2019 Jul 15;35(14):i117–26.

796 34. Long HS, Greenaway S, Powell G, Mallon AM, Lindgren CM, Simon MM. Making sense of
797 the linear genome, gene function and TADs. Epigenetics Chromatin. 2022 Jan 29;15(1):4.

798 35. Das Roy R, Hallikas O, Christensen MM, Renvoisé E, Jernvall J. Chromosomal
799 neighbourhoods allow identification of organ specific changes in gene expression. PLOS
800 Comput Biol. 2021 Sep 10;17(9):e1008947.

801 36. Torelli F, Zander S, Ellerbrok H, Kochs G, Ulrich RG, Klotz C, et al. Recombinant IFN-γ
802 from the bank vole *Myodes glareolus*: A novel tool for research on rodent reservoirs of
803 zoonotic pathogens. Sci Rep. 2018;8(1):1–11.

804 37. Kloch A, Babik W, Bajer A, Siński E, Radwan J. Effects of an MHC-DRB genotype and
805 allele number on the load of gut parasites in the bank vole *Myodes glareolus*. Mol Ecol.
806 2010;19(SUPPL. 1):255–65.

807 38. Migalska M, Sebastian A, Konczal M, Kotlík P, Radwan J. *De novo* transcriptome assembly
808 facilitates characterisation of fast-evolving gene families, MHC class I in the bank vole
809 (*Myodes glareolus*). Heredity. 2017;118(4):348–57.

810 39. Appleton J, Lee KM, Sawicka Kapusta K, Damek M, Cooke M. The heavy metal content of
811 the teeth of the bank vole (*Clethrionomys glareolus*) as an exposure marker of
812 environmental pollution in Poland. Environ Pollut. 2000;110:441–9.

813 40. Gdula-Argasińska J, Appleton J, Sawicka-Kapusta K, Spence B. Further investigation of the
814 heavy metal content of the teeth of the bank vole as an exposure indicator of environmental
815 pollution in Poland. Environ Pollut. 2004;131(1):71–9.

816 41. Yang Z. PAML 4: Phylogenetic Analysis by Maximum Likelihood. Mol Biol Evol. 2007
817 Aug 1;24(8):1586–91.

818 42. Zhang J, Nielsen R, Yang Z. Evaluation of an improved branch-site likelihood method for
819 detecting positive selection at the molecular level. Mol Biol Evol. 2005 Dec;22(12):2472–9.

820 43. Yang Z, Wong WSW, Nielsen R. Bayes Empirical Bayes inference of amino acid sites under
821 positive selection. Mol Biol Evol. 2005 Apr 1;22(4):1107–18.

822 44. Drummond DA, Bloom JD, Adami C, Wilke CO, Arnold FH. Why highly expressed proteins
823 evolve slowly. Proc Natl Acad Sci. 2005 Oct 4;102(40):14338–43.

824 45. Kosiol C, Vinař T, Fonseca RR da, Hubisz MJ, Bustamante CD, Nielsen R, et al. Patterns of
825 positive selection in six mammalian genomes. PLOS Genet. 2008 Aug 1;4(8):e1000144.

826 46. Martincorena I, Luscombe NM. Non-random mutation: The evolution of targeted
827 hypermutation and hypomutation. BioEssays. 2013;35(2):123–30.

828 47. Martincorena I, Roshan A, Gerstung M, Ellis P, Van Loo P, McLaren S, et al. High burden
829 and pervasive positive selection of somatic mutations in normal human skin. Science. 2015
830 May 22;348(6237):880–6.

831 48. Hallikas O, Das Roy R, Christensen MM, Renvoisé E, Sulic AM, Jernvall J. System-level
832 analyses of keystone genes required for mammalian tooth development. J Exp Zoolog B
833 Mol Dev Evol. 2021;336(1):7–17.

834 49. Keränen SVE, Åberg T, Kettunen P, Thesleff I, Jernvall J. Association of developmental
835 regulatory genes with the development of different molar tooth shapes in two species of
836 rodents. Dev Genes Evol. 1998;208(9):477–86.

837 50. Jernvall J, Keränen SVE, Thesleff I. Evolutionary modification of development in
838 mammalian teeth: Quantifying gene expression patterns and topography. Proc Natl Acad
839 Sci. 2000;97(26):14444–8.

840 51. Hughes AL. The evolution of functionally novel proteins after gene duplication. Proc R Soc
841 Lond B Biol Sci. 1997 Jan;256(1346):119–24.

842 52. Wagner A. Selection and gene duplication: A view from the genome. Genome Biol. 2002
843 Apr 15;3(5):reviews1012.1.

844 53. David KT, Oaks JR, Halanych KM. Patterns of gene evolution following duplications and
845 speciations in vertebrates. PeerJ. 2020 Mar 31;8:e8813.

846 54. Copley SD. Evolution of new enzymes by gene duplication and divergence. FEBS J.
847 2020;287(7):1262–83.

848 55. Fisher LW. DMP1 and DSPP: Evidence for duplication and convergent evolution of two
849 SIBLING proteins. Cells Tissues Organs. 2011 Aug;194(2–4):113–8.

850 56. Bouleftour W, Juignet L, Bouet G, Granito RN, Vanden-Bossche A, Laroche N, et al. The
851 role of the SIBLING, bone sialoprotein in skeletal biology — Contribution of mouse
852 experimental genetics. Matrix Biol. 2016 May 1;52–54:60–77.

853 57. Felszeghy S, Módis L, Németh P, Nagy G, Zelles T, Agre P, et al. Expression of aquaporin
854 isoforms during human and mouse tooth development. Arch Oral Biol. 2004 Apr
855 1;49(4):247–57.

856 58. Yoshii T, Harada F, Saito I, Nozawa-Inoue K, Kawano Y, Maeda T. Immunoexpression of
857 aquaporin-1 in the rat periodontal ligament during experimental tooth movement. Biomed
858 Res. 2012;33(4):225–33.

859 59. Zhang X, Zhao J, Li C, Gao S, Qiu C, Liu P, et al. *DSPP* mutation in dentinogenesis
860 imperfecta Shields type II. Nat Genet. 2001 Feb;27(2):151–2.

861 60. de La Dure-Molla M, Philippe Fournier B, Berdal A. Isolated dentinogenesis imperfecta and
862 dentin dysplasia: Revision of the classification. Eur J Hum Genet. 2015 Apr;23(4):445–51.

863 61. Shields ED, Bixler D, El-Kafrawy AM. A proposed classification for heritable human
864 dentine defects with a description of a new entity. Arch Oral Biol. 1973 Apr 1;18(4):543-
865 IN7.

866 62. Sreenath T, Thyagarajan T, Hall B, Longenecker G, D'Souza R, Hong S, et al. Dentin
867 sialophosphoprotein knockout mouse teeth display widened predentin zone and develop
868 defective dentin mineralization similar to human dentinogenesis imperfecta type III. J Biol
869 Chem. 2003 Jul 4;278(27):24874–80.

870 63. Verdelis K, Ling Y, Sreenath T, Haruyama N, MacDougall M, van der Meulen MCH, et al.
871 DSPP effects on *in vivo* bone mineralization. Bone. 2008 Dec 1;43(6):983–90.

872 64. Chen Y, Zhang Y, Ramachandran A, George A. DSPP is essential for normal development
873 of the dental-craniofacial complex. J Dent Res. 2016 Mar 1;95(3):302–10.

874 65. von Marschall Z, Mok S, Phillips MD, McKnight DA, Fisher LW. Rough endoplasmic
875 reticulum trafficking errors by different classes of mutant dentin sialophosphoprotein

(DSPP) cause dominant negative effects in both dentinogenesis imperfecta and dentin dysplasia by entrapping normal DSPP. J Bone Miner Res. 2012;27(6):1309–21.

66. Smith BL, Preston GM, Spring FA, Anstee DJ, Agre P. Human red cell aquaporin CHIP. I. Molecular characterization of ABH and Colton blood group antigens. J Clin Invest. 1994 Sep 1;94(3):1043–9.

67. Jordan IK, Mariño-Ramírez L, Koonin EV. Evolutionary significance of gene expression divergence. Gene. 2005 Jan 17;345(1):119–26.

68. Warnefors M, Kaessmann H. Evolution of the correlation between expression divergence and protein divergence in mammals. Genome Biol Evol. 2013;5(7):1324–35.

69. Jernvall J, Thesleff I. Tooth shape formation and tooth renewal: Evolving with the same signals. Development. 2012;139(19):3487–97.

70. Mitsiadis TA. Role of Islet1 in the patterning of murine dentition. Development. 2003;130(18):4451–60.

71. Charles C, Pantalacci S, Peterkova R, Tafforeau P, Laudet V, Viriot L. Effect of *eda* loss of function on upper jugal tooth morphology. Anat Rec. 2009;292(2):299–308.

72. Zurowski C, Jamniczky H, Graf D, Theodor J. Deletion/loss of bone morphogenetic protein 7 changes tooth morphology and function in *Mus musculus*: Implications for dental evolution in mammals. R Soc Open Sci. 2018 Jan 3;5(1):170761.

73. Cardoso-Moreira M, Halbert J, Valloton D, Velten B, Chen C, Shao Y, et al. Gene expression across mammalian organ development. Nature. 2019 Jul;571(7766):505–9.

74. Finarelli JA, Flynn JJ. Ancestral state reconstruction of body size in the Caniformia (Carnivora, Mammalia): The effects of incorporating data from the fossil record. Syst Biol. 2006;55(2):301–13.

75. Welker F, Collins MJ, Thomas JA, Wadsley M, Brace S, Cappellini E, et al. Ancient proteins resolve the evolutionary history of Darwin's South American ungulates. Nature. 2015 Jun;522(7554):81–4.

76. Warinner C, Korzow Richter K, Collins MJ. Paleoproteomics. Chem Rev. 2022 Aug 24;122(16):13401–46.

77. Zheng GXY, Lau BT, Schnall-Levin M, Jarosz M, Bell JM, Hindson CM, et al. Haplotyping germline and cancer genomes with high-throughput linked-read sequencing. Nat Biotechnol. 2016 Feb;34:303.

78. Marks P, Garcia S, Martinez A, Belhocine K. Resolving the full spectrum of human genome variation using linked-reads. 2017;

79. Weisenfeld NI, Kumar V, Shah P, Church DM, Jaffe DB. Direct determination of diploid genome sequences. Genome Res. 2017;27(5):757–67.

80. Vurture GW, Sedlazeck FJ, Nattestad M, Underwood CJ, Fang H, Gurtowski J, et al. GenomeScope: Fast reference-free genome profiling from short reads. Bioinformatics. 2017 Jul 15;33(14):2202–4.

914 81. Koren S, Walenz BP, Berlin K, Miller JR, Bergman NH, Phillippy AM. Canu: Scalable and
915 accurate long-read assembly via adaptive k-mer weighting and repeat separation. Genome
916 Res. 2017 May 1;27(5):722–36.

917 82. Warren RL. RAILS and Cobbler: Scaffolding and automated finishing of draft genomes
918 using long DNA sequences. J Open Source Softw. 2016 Nov 17;1(7):116.

919 83. Gurevich A, Saveliev V, Vyahhi N, Tesler G. QUAST: Quality assessment tool for genome
920 assemblies. Bioinformatics. 2013 Apr 15;29(8):1072–5.

921 84. Simão FA, Waterhouse RM, Ioannidis P, Kriventseva EV, Zdobnov EM. BUSCO: Assessing
922 genome assembly and annotation completeness with single-copy orthologs. Bioinformatics.
923 2015 Oct 1;31(19):3210–2.

924 85. Cantarel BL, Korf I, Robb SMC, Parra G, Ross E, Moore B, et al. MAKER: An easy-to-use
925 annotation pipeline designed for emerging model organism genomes. Genome Res.
926 2008;18:188–96.

927 86. Campbell MS, Law M, Holt C, Stein JC, Moghe GD, Hufnagel DE, et al. MAKER-P: A tool
928 kit for the rapid creation, management, and quality control of plant genome annotations.
929 Plant Physiol. 2014 Feb 1;164(2):513–24.

930 87. Campbell MS, Holt C, Moore B, Yandell M. Genome annotation and curation using
931 MAKER and MAKER-P. Curr Protoc Bioinforma. 2014 Dec 12;48:4.11.1-4.11.39.

88. Grabherr MG, Haas BJ, Yassour M, Levin JZ, Thompson DA, Amit I, et al. Trinity: Reconstructing a full-length transcriptome without a genome from RNA-Seq data. Nat Biotechnol. 2011 May 15;29(7):644–52.

89. Wheeler TJ, Clements J, Eddy SR, Hubley R, Jones TA, Jurka J, et al. Dfam: A database of repetitive DNA based on profile hidden Markov models. Nucleic Acids Res. 2013 Jan;41(Database issue):D70-82.

90. Caballero J, Smit AFA, Hood L, Glusman G. Realistic artificial DNA sequences as negative controls for computational genomics. Nucleic Acids Res. 2014 Jul;42(12):e99.

91. Hubley R, Finn RD, Clements J, Eddy SR, Jones TA, Bao W, et al. The Dfam database of repetitive DNA families. Nucleic Acids Res. 2016 Jan 4;44(D1):D81–9.

92. Hu J, Zheng Y, Shang X. MiteFinder: A fast approach to identify miniature inverted-repeat transposable elements on a genome-wide scale. In: 2017 IEEE International Conference on Bioinformatics and Biomedicine (BIBM). 2017. p. 164–8.

93. Gremme G, Steinbiss S, Kurtz S. GenomeTools: A comprehensive software library for efficient processing of structured genome annotations. IEEE/ACM Trans Comput Biol Bioinform. 2013 May 1;10(03):645–56.

94. Smit A, Hubley R. RepeatModeler Open-1.0. 2008.

95. Keller O, Kollmar M, Stanke M, Waack S. A novel hybrid gene prediction method employing protein multiple sequence alignments. Bioinformatics. 2011 Mar 15;27(6):757–63.

952 96. Korf I. Gene finding in novel genomes. BMC Bioinformatics. 2004 May 14;5(1):59.

953 97. Campbell MS. compare_annotations_3.2.pl [Internet]. 2015. Available from:
954 https://github.com/mscampbell/Genome_annotation/blob/master/compare_annotations_3.2.
955 pl

956 98. Eilbeck K, Moore B, Holt C, Yandell M. Quantitative measures for the management and
957 comparison of annotated genomes. BMC Bioinformatics. 2009 Feb 23;10(1):67.

958 99. Liu D, Hunt M, Tsai IJ. Inferring synteny between genome assemblies: A systematic
959 evaluation. BMC Bioinformatics. 2018 Jan;19(1):26.

960 100. Emms DM, Kelly S. OrthoFinder: Solving fundamental biases in whole genome
961 comparisons dramatically improves orthogroup inference accuracy. Genome Biol. 2015
962 Aug 6;16(1):157.

963 101. Katoh K, Misawa K, Kuma K ichi, Miyata T. MAFFT: A novel method for rapid multiple
964 sequence alignment based on fast Fourier transform. Nucleic Acids Res. 2002
965 Jul;30(14):3059–66.

966 102. Lefort V, Desper R, Gascuel O. FastME 2.0: A comprehensive, accurate, and fast distance-
967 based phylogeny inference program. Mol Biol Evol. 2015 Oct 1;32(10):2798–800.

968 103. Farrer RA. Synima: A synteny imaging tool for annotated genome assemblies. BMC
969 Bioinformatics. 2017 Nov 21;18(1):507.

970 104. Wang Y, Tang H, DeBarry JD, Tan X, Li J, Wang X, et al. MCScanX: A toolkit for
971 detection and evolutionary analysis of gene synteny and collinearity. Nucleic Acids Res.
972 2012 Apr;40(7):e49.

973 105. Zhao T, Schranz ME. Network approaches for plant phylogenomic synteny analysis. Curr
974 Opin Plant Biol. 2017 Apr 1;36:129–34.

975 106. Zhao T, Holmer R, de Bruijn S, Angenent GC, van den Burg HA, Schranz ME.
976 Phylogenomic synteny network analysis of MADS-Box transcription factor genes reveals
977 lineage-specific transpositions, ancient tandem duplications, and deep positional
978 conservation. Plant Cell. 2017 Jun 1;29(6):1278–92.

979 107. Zhao T, Schranz ME. Network-based microsynteny analysis identifies major differences
980 and genomic outliers in mammalian and angiosperm genomes. Proc Natl Acad Sci. 2019
981 Feb 5;116(6):2165–74.

982 108. Sievers F, Higgins DG. Clustal Omega. Curr Protoc Bioinforma. 2014;48(1):3.13.1-
983 3.13.16.

984 109. Suyama M, Torrents D, Bork P. PAL2NAL: Robust conversion of protein sequence
985 alignments into the corresponding codon alignments. Nucleic Acids Res. 2006 Jul
986 1;34(suppl_2):W609–12.

987 110. Wong WSW, Yang Z, Goldman N, Nielsen R. Accuracy and power of statistical methods
988 for detecting adaptive evolution in protein coding sequences and for identifying positively
989 selected sites. Genetics. 2004 Oct 1;168(2):1041–51.

990 111. Löytynoja A, Vilella AJ, Goldman N. Accurate extension of multiple sequence alignments
991 using a phylogeny-aware graph algorithm. Bioinformatics. 2012 Jul 1;28(13):1684–91.

992 112. Jones DT. Protein secondary structure prediction based on position-specific scoring
993 matrices. J Mol Biol. 1999 Sep 17;292(2):195–202.

994 113. Buchan DWA, Jones DT. The PSIPRED protein analysis workbench: 20 years on. Nucleic
995 Acids Res. 2019 Jul 2;47(W1):W402–7.

996 114. Ewels PA, Peltzer A, Fillinger S, Patel H, Alneberg J, Wilm A, et al. The nf-core
997 framework for community-curated bioinformatics pipelines. Nat Biotechnol. 2020
998 Mar;38(3):276–8.

999 115. Andrews S. FastQC: A quality control tool for high throughput sequence data. [Internet].
1000 2010. Available from: http://www.bioinformatics.babraham.ac.uk/projects/fastqc

1001 116. Martin M. Cutadapt removes adapter sequences from high-throughput sequencing reads.
1002 EMBnet.journal. 2011 May 2;17(1):10–2.

1003 117. Kopylova E, Noé L, Touzet H. SortMeRNA: Fast and accurate filtering of ribosomal RNAs
1004 in metatranscriptomic data. Bioinformatics. 2012 Dec 1;28(24):3211–7.

1005 118. Patro R, Duggal G, Love MI, Irizarry RA, Kingsford C. Salmon provides fast and bias-
1006 aware quantification of transcript expression. Nat Methods. 2017 Apr;14(4):417–9.

1007 119. Love MI, Huber W, Anders S. Moderated estimation of fold change and dispersion for
1008 RNA-seq data with DESeq2. Genome Biol. 2014 Dec 5;15(12):550.

1009 120. Lindblad-Toh K, Garber M, Zuk O, Lin MF, Parker BJ, Washietl S, et al. A high-resolution
1010 map of human evolutionary constraint using 29 mammals. Nature. 2011
1011 Oct;478(7370):476–82.

1012 121. Weyrich A, Schüllermann T, Heeger F, Jeschek M, Mazzoni CJ, Chen W, et al. Whole
1013 genome sequencing and methylome analysis of the wild guinea pig. BMC Genomics. 2014
1014 Nov 28;15(1):1036.

1015 122. Gossmann TI, Ralser M. *Marmota marmota*. Trends Genet. 2020 May;36(5):383–4.

1016 123. Di Palma F, Alföldi J, Johnson J, Berlin A, Gnerre S, Jaffe D, et al. The draft genome of
1017 *Microtus ochrogaster*. Broad Inst [Internet]. 2012; Available from:
1018 https://www.ncbi.nlm.nih.gov/bioproject/72443

1019 124. Mouse Genome Sequencing Consortium, Waterston RH, Lindblad-Toh K, Birney E,
1020 Rogers J, Abril JF, et al. Initial sequencing and comparative analysis of the mouse genome.
1021 Nature. 2002 Dec 5;420(6915):520–62.

1022 125. Di Palma F, Alföldi J, Johnson J, Berlin A, Gnerre S, Jaffe D, et al. The draft genome of
1023 *Jaculus jaculus*. Broad Inst [Internet]. 2012; Available from:
1024 https://www.ncbi.nlm.nih.gov/bioproject/72445

1025 126. Gibbs RA, Weinstock GM, Metzker ML, Muzny DM, Sodergren EJ, Scherer S, et al.
1026 Genome sequence of the Brown Norway rat yields insights into mammalian evolution.
1027 Nature. 2004 Apr;428(6982):493–521.

1028 127. Kolmogorov M, Armstrong J, Raney BJ, Streeter I, Dunn M, Yang F, et al. Chromosome
1029 assembly of large and complex genomes using multiple references. Genome Res. 2018 Nov
1030 1;28(11):1720–32.

1031 128. Lilue J, Doran AG, Fiddes IT, Abrudan M, Armstrong J, Bennett R, et al. Sixteen diverse
1032 laboratory mouse reference genomes define strain-specific haplotypes and novel functional
1033 loci. Nat Genet. 2018 Nov;50(11):1574–83.

1034 129. Couger MB, Arévalo L, Campbell P. A high quality genome for *Mus spicilegus*, a close
1035 relative of house mice with unique social and ecological adaptations. G3
1036 GenesGenomesGenetics. 2018 May 24;8(7):2145–52.

1037 130. Chinese hamster CHOK1GS assembly and gene annotation. Horiz Eagle [Internet]. 2017;
1038 Available from: https://www.ensembl.org/Cricetulus_griseus_chok1gshd/Info/Annotation

1039 131. Di Palma F, Alföldi J, Johnson J, Berlin A, Gnerre S, Jaffe D, et al. The draft genome of
1040 *Mesocricetus auratus*. Broad Inst [Internet]. 2012; Available from:
1041 https://www.ncbi.nlm.nih.gov/bioproject/77669

1042 132. Lassance JM, Hopi Hoekstra. Improved assembly of the deer mouse *Peromyscus*
1043 *maniculatus* genome. Harv Univ Hughes Med Inst [Internet]. 2018; Available from:
1044 https://www.ncbi.nlm.nih.gov/bioproject/494228

1045 133. Fang X, Nevo E, Han L, Levanon EY, Zhao J, Avivi A, et al. Genome-wide adaptive
1046 complexes to underground stresses in blind mole rats *Spalax*. Nat Commun. 2014 Jun
1047 3;5(1):3966.

134. Di Palma F, Alföldi J, Johnson J, Berlin A, Gnerre S, Jaffe D, et al. The draft genome of *Octodon degu*. Broad Inst [Internet]. 2012; Available from: https://www.ncbi.nlm.nih.gov/bioproject/74595

135. Keane M, Craig T, Alföldi J, Berlin AM, Johnson J, Seluanov A, et al. The naked mole rat genome resource: Facilitating analyses of cancer and longevity-related adaptations. Bioinforma Oxf Engl. 2014 Dec 15;30(24):3558–60.

136. Di Palma F, Alföldi J, Johnson J, Berlin A, Gnerre S, Jaffe D, et al. The draft genome of *Chinchilla lanigera*. Broad Inst [Internet]. 2012; Available from: https://www.ncbi.nlm.nih.gov/bioproject/68239

137. V. Federov, Dalen L, Olsen RA, Goropashnaya AV, Barnes BM. The genome of the Arctic ground squirrel *Urocitellus parryii*. Inst Arct Biol [Internet]. 2018; Available from: https://www.ncbi.nlm.nih.gov/bioproject/477386

138. Di Palma F, Alföldi J, Johnson J, Berlin A, Gnerre S, Jaffe D, et al. The draft genome of *Ictidomys tridecemlineatus*. Broad Inst [Internet]. 2012; Available from: https://www.ncbi.nlm.nih.gov/bioproject/61725

139. Schneider VA, Graves-Lindsay T, Howe K, Bouk N, Chen HC, Kitts PA, et al. Evaluation of GRCh38 and de novo haploid genome assemblies demonstrates the enduring quality of the reference assembly. Genome Res. 2017 May 1;27(5):849–64.